Enhancing GEO satellite safety through orbit maintenance using open source software DACEyPy

Michele Maestrini*†

*Politecnico di Milano, Department of Aerospace Science and Technology
Via La Masa 34, 20156, Milan, IT
michele.maestrini@polimi.it

†Corresponding author

Abstract

This work introduces a novel satellite station-keeping (SK) strategy for geostationary Earth orbit using DACEyPy, a Python-based open-source library leveraging differential algebra (DA). DACEyPy enables fast software prototyping for high-order, feedback optimal control through polynomial approximations of orbital dynamics, ensuring robustness and efficiency. The approach is tested on both energy-optimal and fuel-optimal problems, adapting to perturbations in real time with minimal computation. DACEyPy also broadens access to advanced DA methods, supporting mission analysis and control across diverse aerospace applications through an open-source, flexible framework.

1. Introduction

The Geostationary Earth Orbit (GEO) is a distinct orbital zone characterized by circular, equatorial trajectories at an altitude where a satellite's orbital velocity matches the rotational speed of the Earth. This alignment allows the satellite to remain stationary relative to a fixed point on the Earth's surface, enabling ground-based antennas to maintain a continuous and stable communication link. Consequently, GEO is especially advantageous for applications such as weather monitoring and telecommunications.⁵ However, the increasing utilization of this orbital region has resulted in congestion, making it one of the most tightly regulated areas in space due to its high strategic and commercial value. As reported in,⁹ the number of objects occupying GEO is nearing 1000, prompting the Inter-Agency Space Debris Coordination Committee to establish a designated protected region within GEO.¹⁴ Given this rapid growth, active management of operational satellites in GEO is crucial to maintain their assigned positions and to ensure safe operation alongside other spacecraft. To this end, operational GEO satellites execute a sequence of predefined maneuvers known as Station-Keeping (SK). The objective of SK is to avoid collisions and to keep satellites within their allocated latitude and longitude boundaries.²³

1.1 State-of-the-art in Station Keeping Maneuvers Design

The design of Station-Keeping (SK) maneuvers is a well-established topic in the literature. Various approaches are employed depending on the type of thrusters installed on the spacecraft. Impulsive SK, for instance, is a standard procedure in which maneuver plans are calculated on the ground and then transmitted to the satellite in orbit.²² Typically, SK maneuvers are divided into North/South and East/West components to separately manage inclination and longitude control.²³ It is important to note that SK maneuvers are primarily intended to counteract minor orbital drifts. Therefore, they do not demand high levels of thrust and can be effectively carried out using low-thrust electric propulsion systems. When simplifying assumptions are used, analytical SK control laws can be obtained.²⁴ To counteract the effect of their poor accuracy, closed-loop control methods were developed in the past few decades.¹³ In¹⁷ the authors explored a direct optimization method for geostationary SK formulated as a constrained linear quadratic optimal control problem. Alternatively,⁶ introduced a novel formulation of the equations of motion to design SK maneuvers using convex optimization. Finally,¹¹ reconstructs the actual motion of a GEO object using a linearized state-space representation, providing a detailed analysis of the perturbing potentials across various reference frames. This framework enables the formulation of a minimum-fuel geostationary SK problem by incorporating switching system theory and enforcing operational constraints.^{10,12}

This paper will leverage the open source library DACEyPy to develop several optimization strategies for semianalytic SK design. The DACEyPy library, presented in detail in Sec. 2.2, is a Python implementation of Differential

Algebra (DA), a technique that is used to operate in the computer environment directly on Taylor polynomials rather than on floating point numbers. To begin, fundamental concepts regarding the adopted dynamics and DA are introduced in Sec. 2. Then, Sec. 3 provides an overview of the methodology for the proposed SK strategy. Initially, a semi-analytical method for the solution of the energy-optimal control law is introduced in Sec. 3.2. Subsequently, Sec. 3.3 extends the approach to retrieve a minimum fuel solution. The results are reported in Sec. 4. Finally, a summary of the conclusions and suggestions for further developments are presented in 5.

2. Background Concepts and Materials

The GEO orbit is defined as circular and equatorial with a period of 24 h. To describe such dynamics, spherical coordinates can be adopted thanks to the definition of the Earth Centered Earth Fixed (ECEF) frame. In this reference frame one axis (K) points to the North Pole, while the other two rotate with the Earth, and are defined such that $\hat{\mathbf{I}}$ follows the Greenwich Meridian, while $\hat{\mathbf{J}}$ completes the frame.

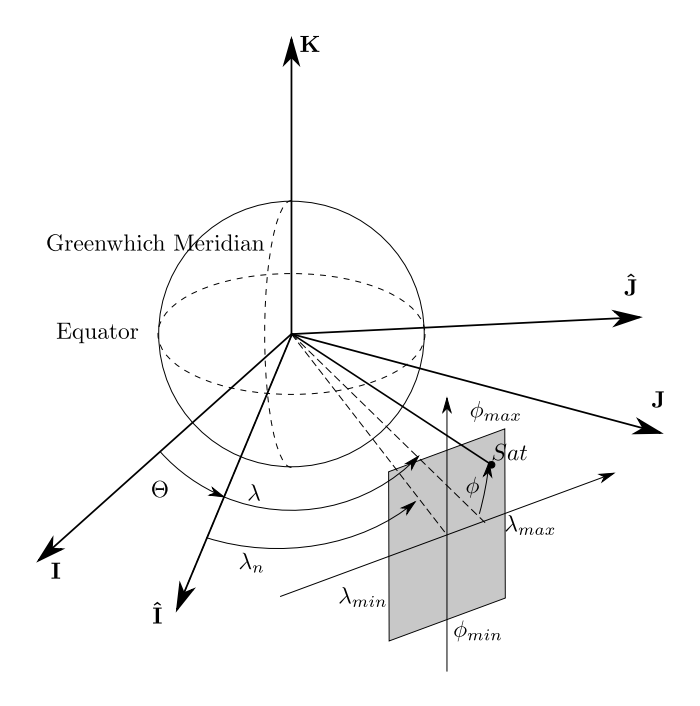


Figure 1: Representation of the ECEF frame.

A set of spherical coordinates can be adopted to describe the motion: r is the distance of the satellite from the Earth center; λ is the longitude of the satellite; while ϕ is the latitude. This set of coordinates allows to describe the nominal unperturbed GEO motion as a fixed point $(r_{GEO}, \lambda_n, \phi_n = 0^\circ)$. If perturbations are present (or a control acceleration), their influence can be computed by taking the gradient of the total potential in spherical coordinates as shown in literature.³ Defining the state $\mathbf{x} = [r \lambda \phi v \dot{\lambda} \dot{\phi}]$ and a control acceleration vector $\mathbf{u} = [u_r, u_\lambda, u_\phi]$, the dynamics is formulated as:

$$\ddot{\mathbf{x}} = \mathbf{f}(\mathbf{x}, \mathbf{u}, t) = \begin{cases} \dot{r} = \dot{r} \\ \dot{\lambda} = \dot{\lambda} \\ \dot{\phi} = \dot{\phi} \\ \dot{v} = -\frac{\mu_E}{r^2} + r\dot{\phi}^2 + r(\dot{\lambda} + \omega_E)^2 \cos \phi^2 + a_r^p(r, \lambda, \phi) + u_r \\ \dot{\lambda} = 2\dot{\phi}(\dot{\lambda} + \omega_E) \tan \phi - 2\frac{v}{r}(\dot{\lambda} + \omega_E) + \frac{1}{r\cos\phi}a_{\lambda}^p(r, \lambda, \phi) + \frac{1}{r\cos\phi}u_{\lambda} \\ \dot{\phi} = -2\frac{v}{r}\dot{\phi} - (\dot{\lambda} + \omega_E)^2 \sin\phi\cos\phi + \frac{1}{r}a_{\phi}^p(r, \lambda, \phi) + \frac{1}{r}u_{\phi} \end{cases}$$

$$(1)$$

with μ_E representing Earth's gravitational constant (i.e., 398600 km³/s²) and a_i^p represent the perturbing accelerations acting on each *i*-th coordinate. The drift from the center of the nominal GEO position is caused by such perturbation.

This work includes the most crucial ones for this orbital regime:²⁶ Earth's nonhomogeneous mass distribution, third-body effects caused by both Sun and Moon, and solar radiation pressure (SRP).

2.1 Basics of Differential Algebra

Differential Algebra (DA)¹⁹ is a framework dedicated to the manipulation —in a computer environment— of high-order Taylor expansions directly, rather than of floating point numbers. In this algebra of polynomials, the operations of integration, derivation, and polynomial inversion are well-defined operations.²

Consequently, if a sufficiently differentiable function $\mathbf{f}(\mathbf{x})$ of m variables is provided, DA can compute its Taylor expansion $\mathcal{M}_f(\delta \mathbf{x})$ up to an arbitrary order n with fixed effort by using DA variables (i.e., $\delta \mathbf{x}$) to perturb the evaluation point \mathbf{x} . DA has several possible applications that can be found in literature, but in this work it was leveraged to obtain polynomial maps of the flow of Ordinary Differential Equations (ODE)¹ and Two-Point Boundary Value Problems (TPBVP). ¹⁵

Every mathematical process relying only on algebraic operations can be computed in DA environment. When this is done the final outcome of the sequence of operations is the arbitrary order expansion of the flow of the process. For example, the ODE $\dot{x} = f(x,t)$ with set initial state x_0 can be integrated using numerical methods to retrieve the Taylor expansion of the ODE flow. In particular, the n^{th} order Taylor expansion of the flow $\mathcal{M}_k(\delta x_0)$ is retrieved at each integration step k if the initial state x_0 is declared as a DA variable $[x_0] = x_0 + \delta x_0$.

Berz and Makino¹⁸ and later DACE²⁰ implemented a version of DA in different programming languages. In this work, we leverage the latter to propose DACEyPy¹, an open-source Python implementation of DACE which is publicly available on GitHub. This library combines the computational efficiency of the DACE compiled core with Python's extensive ecosystem of open-source modules for added flexibility.

2.2 DACEyPy Features

This paper introduces DACEyPy, an open-source Python interface to a DA core written in C. This has been achieved by building on the capabilities of the C++ interface (i.e., DACE) but enhancing its usability and extending its functionality thanks to a more accessible programming language. An overview of the core components and additional features is illustrated in Fig. 2.

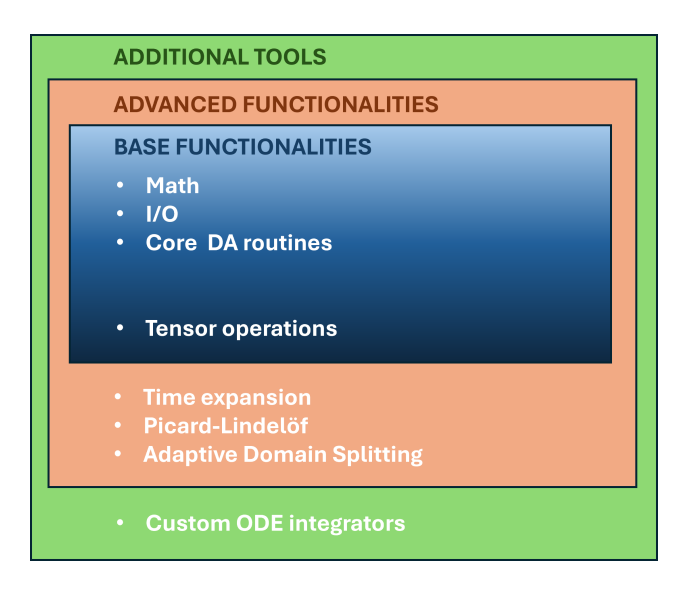


Figure 2: Code scheme for DACEyPy.

Thanks to its Python-based implementation, DACEyPy offers improved accessibility for entry-level programmers and seamless integration with Python's extensive ecosystem, particularly for postprocessing and visualization. Unlike the C++ version, which relies on custom classes for tensor operations, DACEyPy uses standard numpy arrays, eliminating the need for ad-hoc vector and matrix classes. This has been highlighted in Fig. 2: the base functionalities (light blue background) are shared with the C++ implementation, while tensor operations (darker blue) are more naturally supported in DACEyPy through native Python tools.

https://github.com/giovannipurpura/daceypy.git

Beyond ease of use, DACEyPy introduces new capabilities that not present in the original DACE. A key addition is an object-oriented numerical integrator supporting multiple high-order Runge-Kutta schemes with adaptive step sizing. This feature is especially valuable for custom implementations, as DA techniques require full access to the code to correctly operate on DA objects. The integrator is highly configurable, allowing users to define custom dynamics, tolerances, and event-handling functions, and is also modular, supporting the use or development of alternative integration methods.

DACEyPy also brings several advanced DA methods, drawn from current research, into a publicly available framework. For instance, it includes multiple techniques to expand solutions of ODEs as functions of time, either via a modular Picard-Lindeöf operator or through enhancements to the numerical integrator that allow expansion in both initial and final times through appropriate scaling of the dynamics.¹ Furthermore, it provides a flexible framework for adaptive domain splitting (ADS),²⁸ supporting user-defined applications and handling both temporal and state-space splits automatically. All newly introduced features are accompanied by tutorials replicating published state-of-the-art results. Fig. 3 shows and example application of ADS used to propagate initial uncertainty sets subject to standard orbital dynamics.

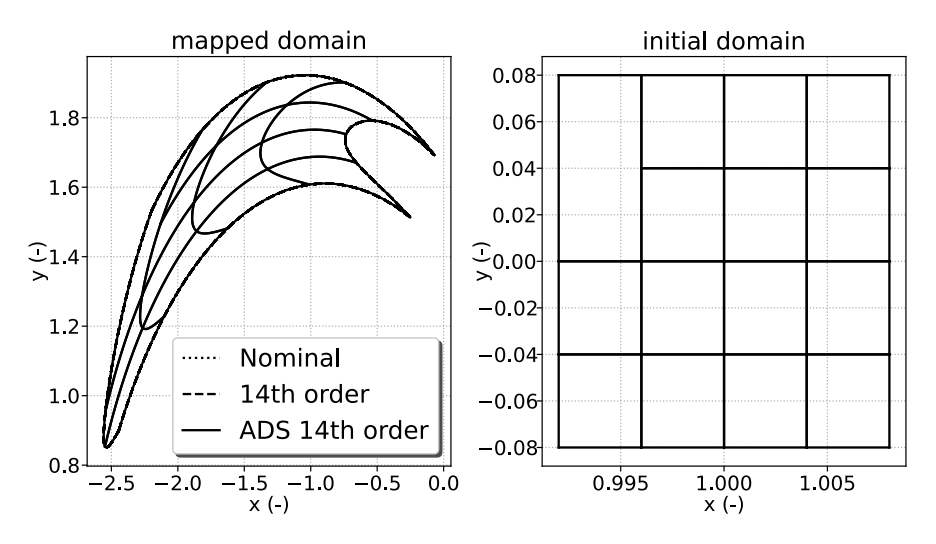


Figure 3: Long term propagation of large initial set of orbital states using ADS.

In addition, another example in Fig. 4 shows how ADS can solve convergence issues for high-order polynomial maps in extremely nonlinear conditions.

3. Station Keeping Approach

In this work, DA is used to implement a SK strategy for GEO orbit. A sequential concept to SK design, similar to methods applied in other in-orbit operations such as hovering and inspection, 21,29 is proposed in this paper. The method consists of a sequence of controlled arcs and uncontrolled drift phases with the aim of keeping a spacecraft within its assigned GEO box. The free drifting phase (FD) owed to orbital perturbations begins from a target state \mathbf{x}_T and lasts until the GEO slot is violated. Then, the satellite is controlled to a new target point \mathbf{x}_T' , from which it will be subject to the next FD phase.

As a consequence, the problem can be split in two main building blocks. First, find the sequence of optimal target points that maximize the free-drift time within the GEO slot, illustrated in Sec. 3.1. Secondly, solve the optimal control problem to reach each of the selected target points in the sequence. This second step includes both an energy-optimal solution (i.e., Sec. 3.2 as well as the expansion of the fuel-optimal one (i.e., Sec. 3.3).

3.1 Selection of target states

The objective of the first step of the optimization is to generate an optimal sequence of targets that reduce the total number of control cycles to a minimum by maximizing the FD duration over a fixed planning horizon. To do so, an iterative optimization procedure is setup.

The first iteration starts from the reference time of the analysis. To initialize the optimization, an analytical initial guess of the state that provides maximum FD according to an approximated dynamic model is provided as in Reference.⁷ Then, MATLAB[®] *fmincon* is used to adjust the optimal initial state of the FD. The optimization scheme

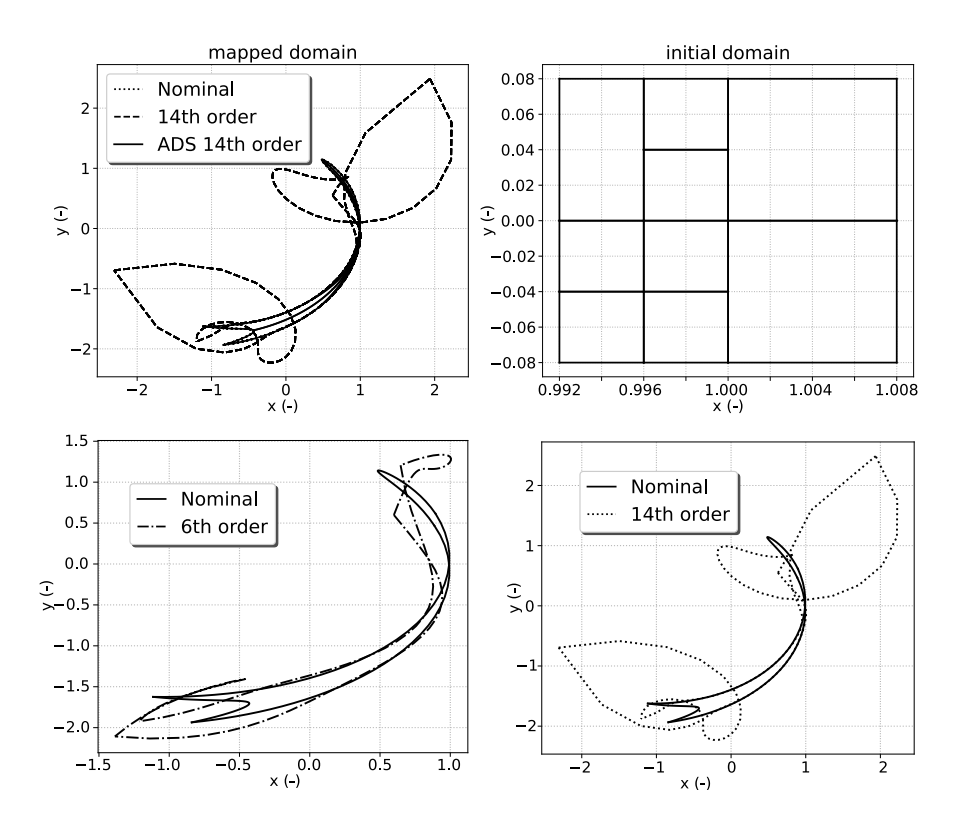


Figure 4: ADS convergence compared to single high-order polynomial maps.

uses an event function to detect violation of the GEO slot boundaries and varies the initial conditions (within the admissible region) to obtain the maximum feasible FD period t_{FD}^{\max} and the optimal target state \mathbf{x}_T . After identifying the target state, the reference time is shifted by $t_{FD}^{\max} + t_C$, where t_C represents the control time, and the optimization procedure is repeated.

Due to the time-varying nature of the perturbations, each optimization will produce a different target state, and the procedure ends once the total time reaches the length of the planning time window $t_{\rm span}$. While this approach implies a significant computational burden, the optimization can be precomputed and stored for later use: this eliminates the need for real-time optimization if the planning horizon is sufficiently long (e.g., 1 year).

This approach was applied for SK in a GEO slot characterized by λ and ϕ bands of 0.1°, using a t_{span} of 1 year and a t_C of 1 day. The SK scenario is set to start on January 1st, 2023. In this case 14 control cycles were retrieved. The duration of the numerical FD stages are reported in Table 5.

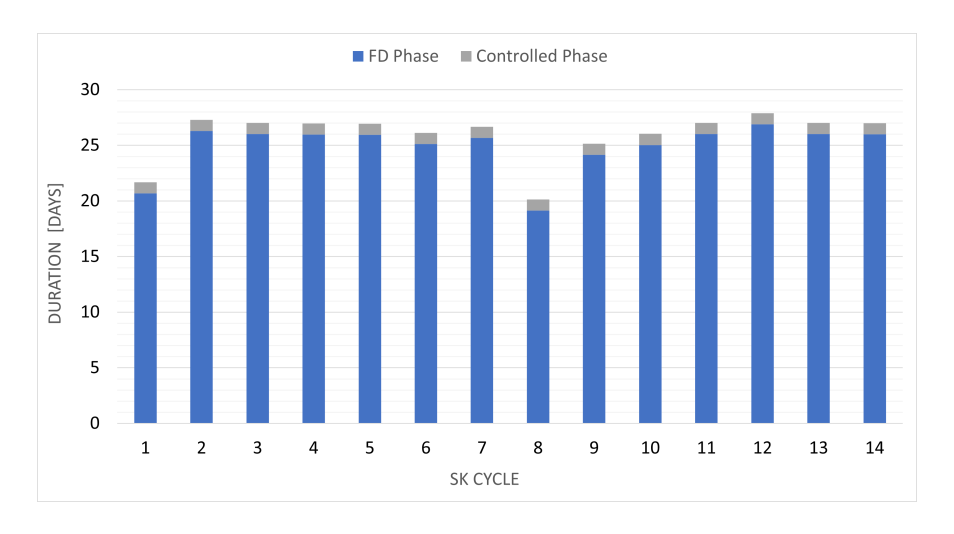


Figure 5: Length of FD and controlled phases from the optimized targets \mathbf{x}_T

3.2 energy-optimal Control Solution

The first method to solve the optimal control problem needed during the control phases is an energy-optimal Control Problem (EOP). Given the dynamical system described by Eqs. 1, the dynamics can be split in free and controlled components as $\mathbf{f}(\mathbf{x}, t, \mathbf{u}) = \hat{\mathbf{f}}(\mathbf{x}, t) + \mathbf{B}(\mathbf{x})\mathbf{u}$. The objective function for this scenario is set to minimize the energy:

$$J = \frac{1}{2} \int_{t_0}^{t_f} \mathbf{u}^{\mathsf{T}} \mathbf{u} \, dt \tag{2}$$

The TPBVP that solves the EOP is obtained through the gradient of the Hamiltonian formulated using the costate I following Reference.⁴ The set of ODEs defining the TPBVP with the prescribed initial and final conditions $\mathbf{x}(t_0) = \mathbf{x}_0$ and $\mathbf{x}(t_f) = \mathbf{x}_T$ becomes:

$$\begin{cases} \dot{\mathbf{x}} = \hat{\mathbf{f}}(\mathbf{x}, t) + \mathbf{B}(\mathbf{x})\mathbf{u} \\ \dot{\mathbf{l}} = -\nabla \hat{\mathbf{f}}(\mathbf{x}, t)^{\mathsf{T}} \mathbf{l} - \nabla (\mathbf{B}(\mathbf{x})\mathbf{u})^{\mathsf{T}} \mathbf{l} \\ \mathbf{u} = -\mathbf{B}_{\mathbf{v}}^{\mathsf{T}}(\mathbf{x})\mathbf{l}_{\mathbf{v}} \end{cases}$$
(3)

where the subscript v represent the part of the vector/array associated only to the velocity components of the state. The solution of this problem is achieved without iterations typical of direct shooting techniques through DA.

The control problem's objective is to find \mathbf{l}_0 that matches matches all the constraints and boundary conditions. Thanks to DA, an arbitrary order n Taylor series expansion of the solution of the optimal control problem with respect to the initial and final states can be performed if the initial states and costates are initialized as DA variables:

$$[\mathbf{x}_0] = \mathbf{x}_0 + \delta \mathbf{x}_0 \tag{4a}$$

$$[\mathbf{l}_0] = \mathbf{l}_0 + \delta \mathbf{l}_0 \tag{4b}$$

Using the techniques described in Sec. 2.1, the solution at t_f is expanded with respect to the starting conditions, as in.⁸

$$\begin{bmatrix} \mathbf{x}_f \\ \mathbf{l}_f \end{bmatrix} = \begin{pmatrix} \mathbf{x}_f \\ \mathbf{l}_f \end{pmatrix} + \begin{pmatrix} \mathcal{M}_{\mathbf{x}_f} \\ \mathcal{M}_{\mathbf{l}_f} \end{pmatrix} \begin{pmatrix} \delta \mathbf{x}_0 \\ \delta \mathbf{l}_0 \end{pmatrix}$$
 (5)

To obtain the variation of initial costates that results in a solution of the EOP, one can subtract the constant parts from this map. Then, the components related to the final state can be extracted and augmented with the identity map I_{x_0} . Afterwards, one can leverage the polynomial map inversion techniques offered natively by DA to obtain:

$$\begin{pmatrix} \delta \mathbf{x}_0 \\ \delta \mathbf{l}_0 \end{pmatrix} = \begin{pmatrix} \mathcal{M}_{\mathbf{x}_f} \\ I_{\mathbf{x}_0} \end{pmatrix}^{-1} \begin{pmatrix} \delta \mathbf{x}_f \\ \delta \mathbf{x}_0 \end{pmatrix} \tag{6}$$

Evaluating the second part of Eq. 6 on the initial and final state deviations it is possible to recover the correction δl_0 that needs to be applied to the initial estimate of the costate to obtain the solution of the optimal control problem.

The method can be further improved using a multifidelity approach. For the given application scenario, it is possible to separate the non-autonomous perturbations from the autonomous ones. The advantage of this approach is that the polynomial expansion of time-independent problems can be precomputed at a high expansion order and can be stored without the need to recompute it for every iteration. In this case, the geopotential dynamics is autonomous and can therefore be used to generate a time-independent high-order polynomial map of the costate. To carry out this expansion, the center of the reference GEO slot (i.e., $\mathbf{x}_n = [r_{GEO}, \lambda_n, \phi_n, 0, 0, 0]$) is chosen as an expansion point. Starting from the ballistic solution characterized by the initial costate $\mathbf{I}_0^{\text{bal}} = \mathbf{0}_{6\times 1}$, the flow can be expanded from the initial epoch of the control t_{Ci} up to $t_{Cf} = t_{Ci} + t_{C}$. However, this can also be approximated as $t_0 = 0$ and $t_f = t_C$ in the autonomous case, and the solution can therefore be used at any time with a control time horizon of t_C . Then, the boundary constraints to match the target state \mathbf{x}_T are imposed as $\delta \mathbf{x}_f = \mathbf{x}_T - \mathbf{x}_f$, together with an initial perturbation defined as $\delta \mathbf{x}_0 = \mathbf{x}_{Ci} - \mathbf{x}_n$, where \mathbf{x}_{Ci} contains the position and velocity of the satellites when the control starts. Using these, one can immediately retrieve the initial costates that solve the autonomous problem $\delta \mathbf{I}_0^{GG}$ through Eq. 6.

Starting from the solution of the reference autonomous problem, one can further correct it to account for timevarying elements of the dynamics (e.g., SRP and third-body). This correction can be executed at lower order since the bulk of nonlinearity is carried by the geopotential perturbation. This choice in turn allows for a significant reduction in computational burden. A first-order DA propagation of the dynamics is requeired from t_{Ci} to t_{Cf} . The initial conditions of state and costate are also set as \mathbf{x}_n and \mathbf{l}_0^{GG} to obtain the linear (L superscript) final state \mathbf{x}_f^L . Consequently, the 1^{st} order feedback of the overall (autonomous and non-autonomous) motion is given by:

$$\begin{cases}
\delta \mathbf{x}_{f}^{L} \\
\delta \mathbf{l}_{f}^{L}
\end{cases} = \begin{bmatrix}
\mathbf{\Phi}_{\mathbf{x}\mathbf{x}} & \mathbf{\Phi}_{\mathbf{x}\mathbf{l}} \\
\mathbf{\Phi}_{\mathbf{l}\mathbf{x}} & \mathbf{\Phi}_{\mathbf{l}\mathbf{l}}
\end{bmatrix} \begin{cases}
\delta \mathbf{x}_{0}^{L} \\
\delta \mathbf{l}_{0}^{L}
\end{cases} \tag{7}$$

$$\delta \mathbf{l}_0^L = \mathbf{\Phi}_{\mathbf{x}\mathbf{l}}^{-1} [\delta \mathbf{x}_f^L - \mathbf{\Phi}_{\mathbf{x}\mathbf{x}} \delta \mathbf{x}_0^L]$$
 (8)

with $\delta \mathbf{x}_f^L = \mathbf{x}_T - \mathbf{x}_f^L$ and $\delta \mathbf{x}_0^L = \delta \mathbf{x}_0$. Since the propagation is only carried out linearly, the polynomial map notation of Eq. 5 is here abandoned in favor of the classic State Transition Matrix (STM) notation $\mathbf{\Phi}$. The final control action can be determined by:

$$\mathbf{l_0} = \mathbf{l}_0^{GG} + \delta \mathbf{l}_0^L \tag{9}$$

3.3 Fuel-optimal Control Expansion

Once the energy-optimal solution is available, the reference solution of the corresponding fuel-optimal problem is obtained via numerical continuation using the energy-optimal solution as an initial guess to ease convergence. Subsequently, DA techniques are developed to build up a robust control trajectory capable of counteracting potential uncertainties or additional perturbations that allow to avoid costly recomputation of optimal control solutions.

Following the EOP formulation in Sec. 3.2, the equations can be modified to deal with this different control problem. Once the propulsion system has been characterized by its specific impulse I_{sp} and its maximum thrust T_{max} , the spacecraft mass variation due to propellant consumption can be expressed with a 1st order ODE that is added to Eq. 1:

$$\begin{cases} \dot{\mathbf{x}} = \mathbf{f}(\mathbf{x}, \hat{\boldsymbol{\alpha}}, u, t) = \tilde{\mathbf{f}}(\mathbf{x}, t) + \frac{T_{max}}{m} u \mathbf{B}(\mathbf{x}) \hat{\boldsymbol{\alpha}} \\ \dot{m} = -\frac{T_{max}}{I_{sp}g_0} u \end{cases}$$
(10)

where u is a throttle factor $\in [0, 1]$, whereas the thrust direction is defined as $\hat{\alpha} = [\alpha_r, \alpha_\lambda, \alpha_\phi]$.

The formulation of the solution to this problem can be derived as in²⁵ starting with the definition of the objective function:

$$J = \frac{T_{max}}{I_{sp}g_0} \int_{t_{Ci}}^{t_{Cf}} u \, dt \tag{11}$$

As in the previous section, this can be used to retrieve a TPBVP subject to initial and final constraints $\mathbf{x}(t_0) = \mathbf{x_0}$ and $\mathbf{x}(t_f) = \mathbf{x}_T$ but with the added transversality condition $l_m(t_f) = 0$ since the final mass is unconstrained. The optimality conditions are obtained with the Pontryagin Maximum Principle²⁷ as:

$$\hat{\alpha} = -\frac{\mathbf{B}_{\mathbf{v}}^{\top}(\mathbf{x})\mathbf{I}_{\mathbf{v}}}{\left\|\mathbf{B}_{\mathbf{v}}^{\top}(\mathbf{x})\mathbf{I}_{\mathbf{v}}\right\|}$$
(12)

$$\hat{\boldsymbol{\alpha}} = -\frac{\mathbf{B}_{\mathbf{v}}^{\top}(\mathbf{x})\mathbf{I}_{\mathbf{v}}}{\left\|\mathbf{B}_{\mathbf{v}}^{\top}(\mathbf{x})\mathbf{I}_{\mathbf{v}}\right\|}$$

$$\begin{cases} u = 0 & if \ \rho > 0 \\ u = 1 & if \ \rho < 0 \end{cases}$$
(12)

with switching function

$$\rho = 1 - \frac{I_{sp}g_0}{m} \|\mathbf{B}_{\mathbf{v}}^{\mathsf{T}}(\mathbf{x})\mathbf{l}_{\mathbf{v}}\| - l_m$$
 (14)

The solution to this problem gives rise to the standard bang-bang discontinuous structure of the control profile characteristic of fuel-optimal problems. In this paper this solution is achieved numerically from the energy-optimal solution through the continuation procedure presented in.¹⁶

When additional perturbations or uncertainties are present, the spacecraft deviates from the computed reference trajectory. As a result of this deviation, the onboard numerical control law cannot be applied as originally planned, and the solution would typically need to be recomputed. To avoid this extra step and instead determine a robust, accurate, and optimal correction that can be implemented onboard, DA techniques can be employed once again. These techniques provide the necessary adjustments to the initial costates and the switching times of the controls. This can be attained by following the procedure outlined in, ¹⁶ whose main steps we recall for convenience.

1. The states, costates, and first switching time are initialized as DA variables about $[\mathbf{x}_0] = \mathbf{x}_{Ci} + \delta \mathbf{x}_0$, $[\mathbf{l}_0] = \mathbf{l}_0^{FOP} + \delta \mathbf{l}_0$, and $[t_{s,1}] = t_{s,1} + \delta t_{s,1}$.

2. The controlled dynamics are propagated according to the reference solution from t_{Ci} to $[t_{s,1}]$: at the end of this expansion, the polynomial map regarding the state (i.e., $[\mathbf{x}_1]$ and $[m_1]$) and costate (i.e., $[\mathbf{l}_1]$ and $[l_{m_1}]$) at the first switch are available as functions of the initialized DA variables. By substituting these maps in the switching function of Eq. 14 its expansion can be obtained:

$$[\rho_1] = 0 + \delta \rho_1 = 1 - \frac{I_{sp}g_0}{[m_1]} \left\| \mathbf{B}_{\mathbf{v}}([\mathbf{x}_1])^{\mathsf{T}} [\mathbf{I}_{\mathbf{v}_1}] \right\| - [l_{m_1}]$$

$$(15)$$

3. To retrieve the switching time correction as a function of initial state and costate variation it is possible to build and invert the following map, while imposing the resulting switching condition is still satisfied as $\delta \rho_1 = 0$:

$$\begin{pmatrix}
\delta \rho_{1} \\
\delta \mathbf{x}_{0} \\
\delta \mathbf{l}_{0} \\
\delta l_{m_{0}}
\end{pmatrix} = \begin{pmatrix}
\mathcal{M}_{\rho_{1}} \\
I_{\mathbf{x}_{0}} \\
I_{\mathbf{l}_{0}} \\
I_{l_{m_{0}}}
\end{pmatrix} \begin{pmatrix}
\delta \mathbf{x}_{0} \\
\delta \mathbf{l}_{0} \\
\delta l_{m_{0}} \\
\delta t_{s,1}
\end{pmatrix} \tag{16}$$

4. Finally, extracting the last row of the inverse polynomial map it is possible to have:

$$[t_{s,1}] = t_{s,1} + \delta t_{s,1} = t_{s,1} + \mathcal{M}_{t_{s,1}}^{\rho_1 = 0}(\delta \mathbf{x}_0, \delta \mathbf{l}_0, \delta l_{m_0})$$
(17)

The same map can be substituted inside the expansion of state and costate to retrieve the expansion only as function of initial states and costates variation $[\mathbf{x}_1] = \mathbf{x}_1 + \mathcal{M}_{x_1}(\delta \mathbf{x}_0, \delta \mathbf{l}_0, \delta l_{m_0}, \mathcal{M}_{t_{s,1}}^{\rho_1=0}(\delta \mathbf{x}_0, \delta \mathbf{l}_0, \delta l_{m_0}))$ and $[\mathbf{l}_1] = \mathbf{l}_1 + \mathcal{M}_{l_1}(\delta \mathbf{x}_0, \delta \mathbf{l}_0, \delta l_{m_0}, \mathcal{M}_{t_{s,1}}^{\rho_1=0}(\delta \mathbf{x}_0, \delta l_0, \delta l_{m_0}))$.

5. At this point, the procedure can restart from step 1, initializing the second control switching time as a DA variable $[t_{s,2}] = t_{s,2} + \delta t_{s,2}$ and propagating $[\mathbf{x}_1]$ and $[\mathbf{l}_1]$ at the previous switch from $[t_{s,1}]$ to $[t_{s,2}]$. The process continues for the whole bang-bang sequence until the last switching time $[t_{sf}]$ is retrieved only as a function of the initial states and costates:

$$t_{s,i} = t_{s,i} + M_{\rho_i = 0}(\delta \mathbf{x_0}, \delta \mathbf{l_0}, \delta l_{m_0})$$
(18)

6. The last segment of the sequence going from $[t_{sf}]$ to t_{Cf} is expanded as in Step 2 to obtain $[\mathbf{x}_f] = \mathbf{x}_f + \mathcal{M}_{x_f}(\delta \mathbf{x}_0, \delta \mathbf{l}_0, \delta l_{m_0})$ and $[\mathbf{l}_f] = \mathbf{l}_f + \mathcal{M}_{l_f}(\delta \mathbf{x}_0, \delta \mathbf{l}_0, \delta l_{m_0})$.

At this point, it is possible to build and invert the square extended polynomial map:

$$\begin{pmatrix}
\delta \mathbf{x}_{0} \\
\delta \mathbf{x}_{f} \\
\delta l_{m_{f}}
\end{pmatrix} = \begin{pmatrix}
I_{\mathbf{x}_{0}} \\
\mathcal{M}_{\mathbf{x}_{f}} \\
\mathcal{M}_{l_{m_{f}}}
\end{pmatrix} \begin{pmatrix}
\delta \mathbf{x}_{0} \\
\delta l_{0} \\
\delta l_{m_{0}}
\end{pmatrix}$$
(19)

The initial guess of the costates can finally be obtained by substituting the boundary conditions $\delta \mathbf{x}_f = [\mathbf{x}_f] - \mathbf{x}_T$ and $\delta l_{mf} = 0$ in the inverse of this polynomial map.

4. Numerical Results

The numerical results obtained by running the energy-optimal multifidelity control solution and the fuel-optimal one for 1 year of SK operations are reported here. The parameters adopted for the satellite are reported in Table 1.

The sequence of target points is selected according to the results of Sec. 3.1. First, the numerical exact solution is obtained with a single shooting method implemented in Python and it is used as the benchmark. The results obtained from the reference solution for 1 year of SK operations are reported in Fig. 6.

The box constraint is violated during the controlled arcs since path constraint are not imposed during control.

Parameter	Value
m [kg]	3000
A_s [m ²]	100
C_r	1.5
λ_n [deg]	60 E
ϕ_n [deg]	0
r_n [km]	42165.8
I_{sp} [s]	3800
T_{max} [N]	0.33

Table 1: Satellite properties

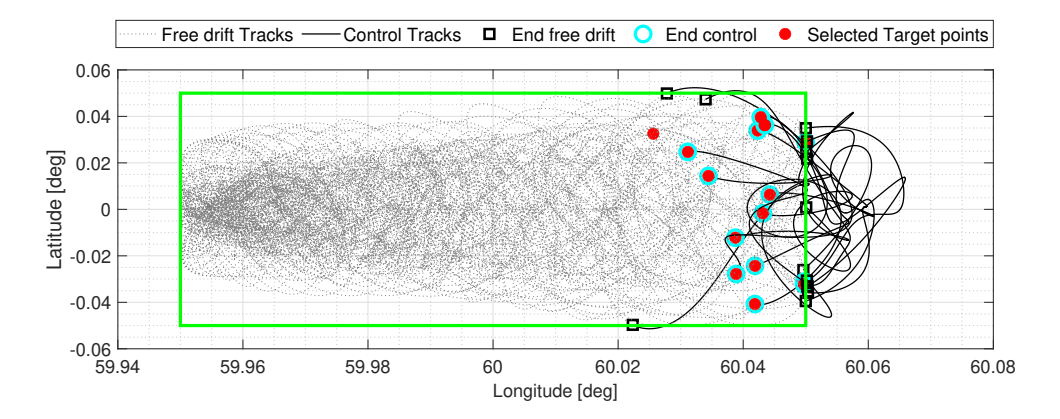


Figure 6: Groundtrack of the GEO satellite following the nominal numerical shooting solution.

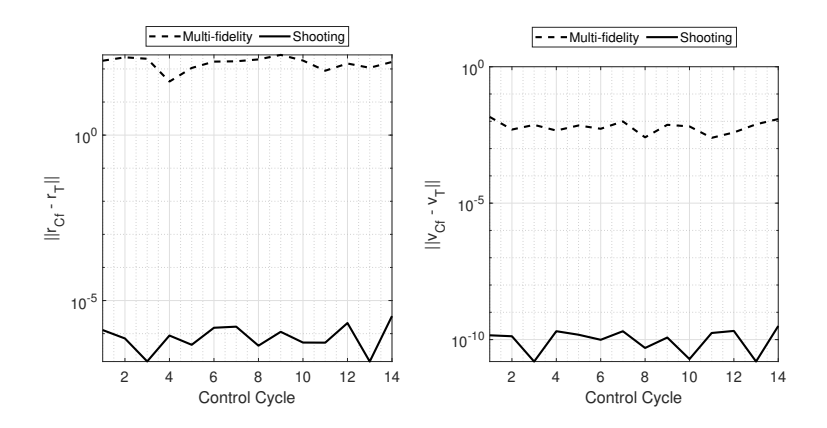


Figure 7: Target states matching error.

4.1 Energy-optimal Control Results

For the multifidelity approach, a 4^{th} order DA expansion of the autonomous system dynamics is precomputed and stored. The outcome of the application of this method is presented in Fig. 8. As can be better observed in Fig. 9, the SK constraints are infringed by approximately 0.025° also on the western edge of the GEO assigned slot due to the small but non-negligible error in final target matching reported in Fig. 7.

To reduce this violation, one can shorten the control time horizon at the cost of increased fuel consumption. Alternatively, one can consider a safety factor in the GEO slot boundaries, which may cause a reduction in FD time, and may consequently reduce the overall optimality of the strategy.

To conclude this section, an analysis on the time and fuel cost for these algorithms is presented. This analysis is performed using Python on an Intel Core i7-1065G7 1.50 GHz, running Windows 11 Home 64 bit. Fig. 10 highlights the efficiency of the multifidelity method in obtaining a solution in a timely fashion.

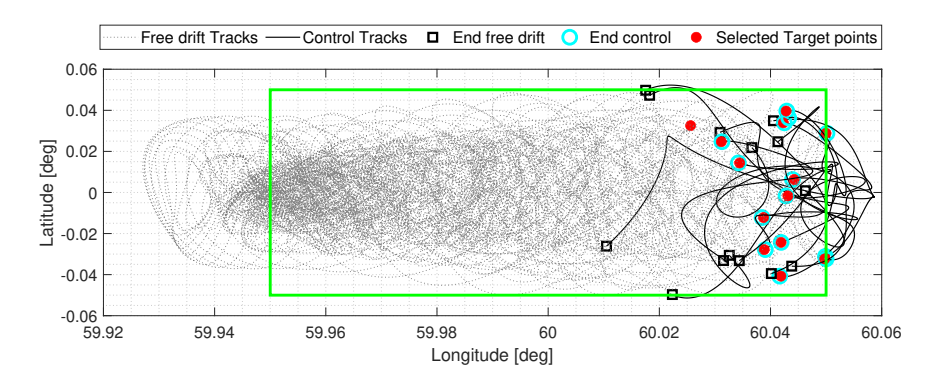


Figure 8: Groundtrack of the GEO satellite adopting the multifidelity method for 1 year of SK.

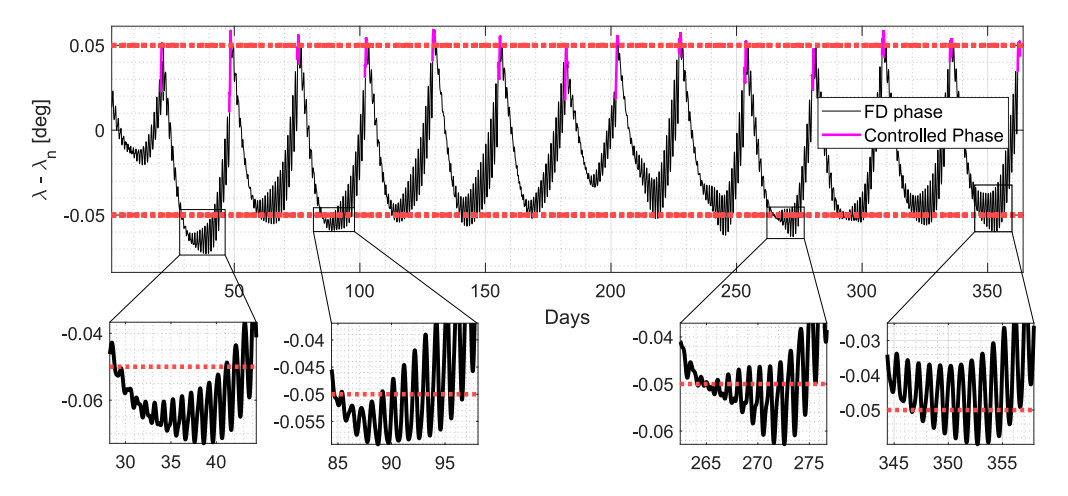


Figure 9: Longitude evolution for the multifidelity energy-optimal method.

The multifidelity control approach is much faster than the numerical shooting reference. In fact, the time-independent map can be precomputed and used onboard for every control cycle (i.e., the time for its computation is not included in this figure). It is clear from Fig. 10 that the application of the high-order autonomous map together with the integration and evaluation of the STM takes on average less than one second. The total computation cost is reported together with the mass and Δv budget for 1 year SK in Table 2.

	Shooting	Multifidelity
$\mathbf{M_b}[kg]$	5.586	5.858
$\Delta \mathbf{v} [m/s]$	69.404	72.787
Total Computational Time [s]	24.094	12.217

Table 2: Total costs metrics for 1 year of SK operations

4.2 Fuel-optimal Control Results

The solution of the fuel-optimal control problem is numerically intensive; therefore, it is desirable to do it as rarely as possible. In case a fuel-optimal reference guidance is obtained with a numerical continuation method presented in Sec. 3.3, expanding it with DA allows some flexibility to variations of initial conditions without having to recompute the reference.

The entire 1 year SK strategy described in the previous section is translated to fuel-optimal structure using the method described in. 16 The fuel-optimal numerical reference retrieves a total mass budget of 4.893 kg/year, and a cumulative Δv of 60.846 m/s/year. As expected, both of these figures are below those obtained using the energy-optimal control. Every cycle has its own switching sequence with different number of commutations and thrust duration, as can be seen in Fig. 11.

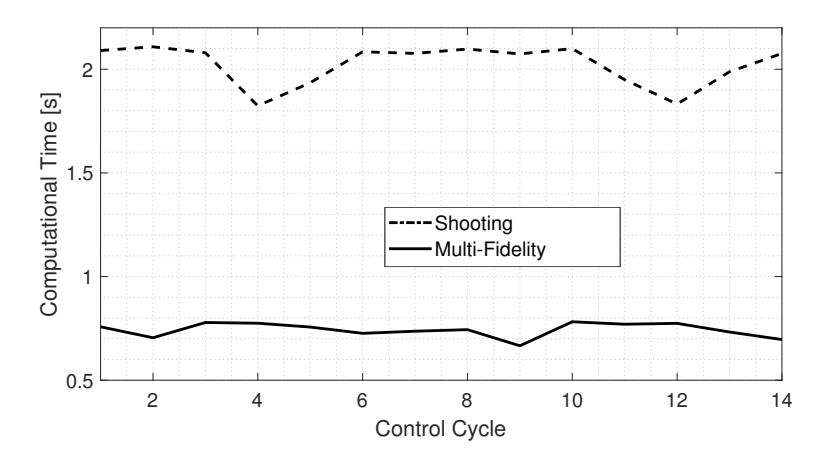


Figure 10: Computational Times.

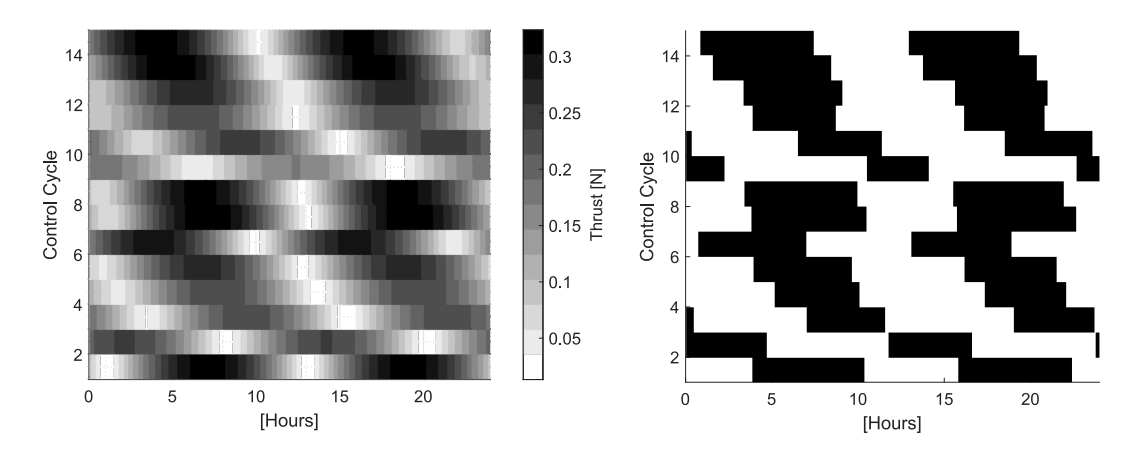


Figure 11: Control Thrust in a Year SK using energy-optimal control (left) and fuel-optimal control (right).

Then, each of the 14 fuel-optimal control strategies is expanded to the second order according to the procedure described in Sec. 3.3. These polynomial maps can help to obtain a robust controller capable of reacting to small initial state variation while enforcing the bang-bang control structure typical of fuel-optimal problems. Secondly, they allow for quick estimation of the impact of variations in key system parameters. For example, it would be possible to use this approach to investigate the impact of varying solar reflection coefficient.

In this work, this method was used to test the effect of navigation uncertainties. For each initial time of the controlled phases during the SK window, a diagonal position covariance matrix \mathbf{P}_i is generated using a range of standard deviations for σ_r , σ_ϕ and σ_l . 100 random samples are then taken from these distributions as initial state variations $\delta \mathbf{x}_0 = \delta \mathbf{x}_{Ci}$ for each maneuver phase. These are substituted in the control adaptation equation described in Sec. 3.3 to obtain corrected controls. For every possible deviation from the initial nominal point, a new optimal bang-bang profile arises. Fig. 12 highlights how the throttle u changes for different samples in the same control phase.

Then, it is possible to obtain an envelope of fuel mass for each maneuver. The results of this sensitivity analysis are presented in Table 3.

5. Conclusions

This paper presented an open-source software DACEyPy and its application to solve the SK problem in GEO. The SK strategy outlined in this paper was designed to counteract drifts resulting from perturbing forces affecting the GEO satellites. The analysis focuses on the most impactful disturbance sources typical of this regime. The proposed algorithm improves fuel efficiency by reducing the frequency of control maneuvers and increasing the duration of uncontrolled motion, taking advantage of natural FD dynamics.

The algorithm is structured into two main parts. The first one, presented in Sec. 3.1, focuses on computing

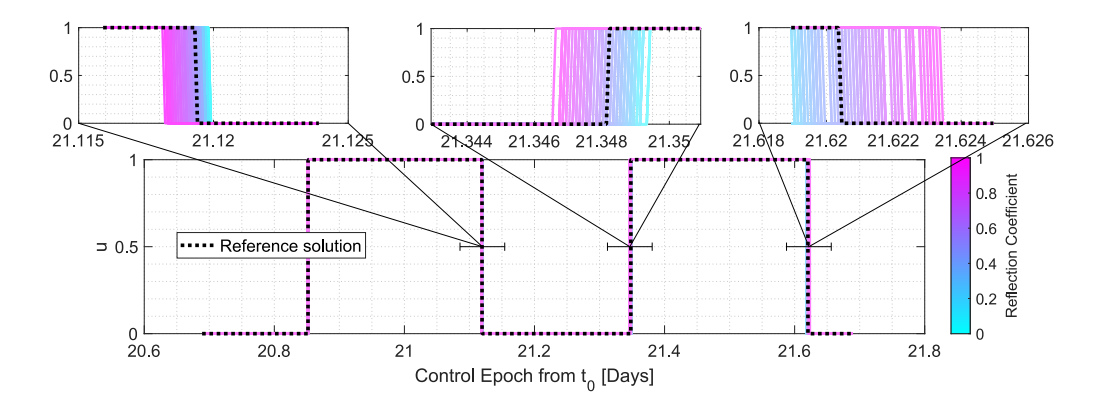


Figure 12: Control Profile Variation

		Radial Uncertainty		
		$\sigma_r = 100 \text{ km}$	$\sigma_r = 10 \text{ km}$	$\sigma_r = 1 \text{ km}$
Angular Uncertainty	$\sigma_{\phi} = \sigma_l = 0.05^{\circ}$	1.84%	1.26%	1.10%
	$\sigma_{\phi} = \sigma_l = 0.01^{\circ}$	1.48%	0.29%	0.19%
	$\sigma_{\phi} = \sigma_l = 0.005^{\circ}$	0.93%	0.20%	0.11%

Table 3: Fuel mass variation for 1 year SK operations assuming different uncertainty levels.

optimized targets that define an overall optimal strategy for long SK durations. In the second one, optimal control solutions to both energy- and fuel-optimal problems are described. For the solution of the energy-optimal problem, a multifidelity approach is employed, using a high-order map of the autonomous dynamics that is precomputed and stored for more efficient use. Whenever necessary, a linear correction term accounting for non-autonomous dynamics can be computed directly on the satellite. However, the fuel-optimal solution is based on a numerical continuation scheme starting from the energy-optimal solution. Then, this reference solution can be expanded using a DA technique that expresses switching times as a function of initial state variations. This feature helps quantify the impact of modeling inaccuracies or navigation errors on the total SK mass budget, enhancing the overall reliability of SK operations.

Despite promising results, the proposed method still presents some issues. One of the main problems is the violation of the SK boundaries for the multifidelity method, which stems from the absence of path constraints in the optimal control problem and from the lack of accuracy in the solution. Also, the methodology developed in this work could be translated to other similar but interesting orbital regimes, such as the aerostationary orbit of Mars.

6. Acknowledgments

The author gratefully acknowledges Giovanni Purpura for his valuable support in maintaining the DACEyPy open-source repository.

References

- [1] R. Armellin, P. Di Lizia, F. Bernelli-Zazzera, and M. Berz. Asteroid close encounters characterization using differential algebra: the case of apophis. *Celestial Mechanics and Dynamical Astronomy*, 107(4):451–470, Aug 2010.
- [2] M. Berz. High-order computation and normal form analysis of repetitive systems. *AIP Conference Proceedings*, 249(1):456–489, 03 1992.
- [3] E. Bois. First-order accurate theory of perturbed circular motion. *Celestial Mechanics and Dynamical Astronomy*, 58(2):125–138, Feb 1994.

- [4] A.E. Bryson. *Applied Optimal Control: Optimization, Estimation and Control*, chapter 2, pages 65–69. CRC Press, 1975.
- [5] Christian Circi, Emiliano Ortore, Carlo Ulivieri, and Tommaso Adamo. Possible alternative to geostationary earth orbit. *Journal of Guidance, Control, and Dynamics*, 38(3):534–539, 2015.
- [6] Frederik J. de Bruijn, Stephan Theil, Daniel Choukroun, and Eberhard Gill. Geostationary satellite station-keeping using convex optimization. *Journal of Guidance, Control, and Dynamics*, 39(3):605–616, 2016.
- [7] Andrea De Vittori, Gabriele Dani, Pierluigi Di Lizia, and Roberto Armellin. Numerically efficient low thrust collision avoidance maneuver design in geo regime with equinoctial orbital elements. In 2nd NEO and Debris Detection Conference, page 61, 2023.
- [8] P. Di Lizia, R. Armellin, F. Bernelli-Zazzera, and M. Berz. High order optimal control of space trajectories with uncertain boundary conditions. *Acta Astronautica*, 93:217–229, 2014.
- [9] ESA Space Debris Office. Esa's annual space environment report, gen-db-log-00288-ops-sd, 2024.
- [10] C. Gazzino, C. Louembet, D. Arzelier, N. Jozefowiez, D. Losa, C. Pittet, and L. Cerri. Integer programming for optimal control of geostationary station keeping of low-thrust satellites. *IFAC-PapersOnLine*, 50(1):8169–8174, 2017. 20th IFAC World Congress.
- [11] Clement Gazzino. Dynamics of a geostationary satellite. HAL science ouverte, 12 2017. Research Report, Rapport LAAS n° 17432, LAAS-CNRS, 2nd Edition.
- [12] Clément Gazzino, Denis Arzelier, Luca Cerri, Damiana Losa, Christophe Louembet, and Christelle Pittet. A three-step decomposition method for solving the minimum-fuel geostationary station keeping of satellites equipped with electric propulsion. *Acta Astronautica*, 158:12–22, 2019.
- [13] Mauricio M. Guelman. Geostationary satellites autonomous closed loop station keeping. *Acta Astronautica*, 97:9–15, 2014.
- [14] IADC. Space debris mitigation guidelines, iadc-02-01 rev 4., 2025.
- [15] P. Di Lizia, R. Armellin, and M. Lavagna. Application of high order expansions of two-point boundary value problems to astrodynamics. *Celestial Mechanics and Dynamical Astronomy*, 102(4):355–375, Dec 2008.
- [16] P. Di Lizia, R. Armellin, A. Morselli, and F. Bernelli-Zazzera. High order optimal feedback control of space trajectories with bounded control. *Acta Astronautica 94, Issue 1: 383-394*, 2014.
- [17] D. Losa, M. Lovera, R. Drai, T. Dargent, and J. Amalric. Electric station keeping of geostationary satellites: a differential inclusion approach. In *Proceedings of the 44th IEEE Conference on Decision and Control*, pages 7484–7489, 2005.
- [18] Kyoko Makino and Martin Berz. Cosy infinity version 9. *Nuclear Instruments and Methods in Physics Research Section A: Accelerators, Spectrometers, Detectors and Associated Equipment*, 558(1):346–350, 2006. Proceedings of the 8th International Computational Accelerator Physics Conference.
- [19] Berz Martin. Chapter 2 differential algebraic techniques. In Peter Hawkes, editor, *Modern Map Methods in Particle Beam Physics*, volume 108 of *Advances in Imaging and Electron Physics*, pages 81–117. Elsevier, 1999.
- [20] Mauro Massari and Alexander Wittig. The differential algebra computational toolbox, 2018.
- [21] J. C. Sanchez, C. Louembet, F. Gavilan, and R. Vazquez. Event-based impulsive control for spacecraft rendezvous hovering phases. *Journal of Guidance, Control, and Dynamics*, 44(10):1794–1810, 2021.
- [22] Shashi Kant Shrivastava. Orbital perturbations and stationkeeping of communication satellites. *Journal of Space-craft and Rockets*, 15(2):67–78, 1978.
- [23] E.M. Soop. Handbook of Geostationary Orbits. Space Technology Library. Springer Netherlands, 2010.
- [24] A.A. Sukhanov and A.F.B.A. Prado. On one approach to the optimization of low-thrust station keeping manoeuvres. *Advances in Space Research*, 50(11):1478–1488, 2012.

- [25] F. Topputo and C. Zhang. Survey of direct transcription for low-thrust space trajectory optimization with applications. *Abstract and Applied Analysis*, vol. 2014, Article ID 851720, 15 pages, 2014.
- [26] D.A. Vallado. Fundamentals of Astrodynamics and Applications. Springer, 3 edition, 2007.
- [27] Yang Wang and Francesco Topputo. Indirect optimization of fuel-optimal many-revolution low-thrust transfers with eclipses. *IEEE Transactions on Aerospace and Electronic Systems*, 59(1):39–51, 2023.
- [28] Alexander Wittig, Pierluigi Di Lizia, Roberto Armellin, Kyoko Makino, Franco Bernelli-Zazzera, and Martin Berz. Propagation of large uncertainty sets in orbital dynamics by automatic domain splitting. *Celestial Mechanics and Dynamical Astronomy*, 122(3):239–261, Jul 2015.
- [29] Chuncheng Zhao, Michele Maestrini, and Pierluigi Di Lizia. Low-thrust optimal control of spacecraft hovering for proximity operations. *Journal of Guidance, Control, and Dynamics*, 47(7):1457–1469, 2024.